PHYSICAL REVIEW B VOLUME 36, NUMBER 12 15 OCTOBER 1987-II

Inelastic phonon scattering in LaF_3 by resonant Raman processes

S. S. Yom,* R. S. Meltzer, and J. E. Rives
Department of Physics and Astronomy, University of Georgia, Athens, Georgia 30602
(Received 11 May 1987)

Resonant Raman scattering is observed to reduce the lifetime of 23-cm^{-1} acoustic phonons in LaF_3 from 600 nsec to a minimum of 125 nsec. A monoenergetic nonequilibrium distribution of phonons is optically produced during relaxation among the crystal-field components of the $^1D_2$ excited state of Pr^{3+} ions present as impurities. The phonon lifetime is measured from the decay of the Pr^{3+} hot luminescence. Resonant scattering is identified by the reduction in the lifetime when the ground-state transitions of co-doped Dy^{3+} ions are tuned into resonance with the phonons by a magnetic field. The temporal behavior of the hot luminescence as a function of magnetic field is analyzed with a set of coupled rate equations for the relevant states of the Pr^{3+} and Dy^{3+} ions as well as the initial and scattered phonon energy packets. We consider in the model anharmonic decay, Raman scattering, and spatial transport limited by the elastic and inelastic scattering of the phonons. We numerically solve the rate equations using known and estimated values of the various parameters. The results describe the experiments well with reasonable values of the unknown parameters.

I. INTRODUCTION

At high temperatures, where there are a large number of high-frequency phonons available, Raman processes often dominate the relaxation of electronic states of ions in solids. Although most of the phonons are nonresonant with the electronic transitions on the impurity ion, with correspondingly small Raman scattering cross sections, the presence of so many phonons results in a large contribution to the relaxation. However, even at relatively low temperatures (~ 5 K), Raman processes can become dominant when the impurity ion has a transition energy which is resonant with a portion of the available phonons (Orbach process). For those phonons, which are in resonance with the electronic transition of the ion, the Raman process can dominate the relaxation of the phonons as well. In this paper, we obtain such a situation when a monoenergetic nonequilibrium distribution of phonons is brought into resonance with the low-lying transitions of an impurity ion by tuning with a magnetic field. We observe a large reduction of the phonon lifetime, which we attribute to inelastic Raman scattering from these resonances.

The important role of Raman scattering in controlling the dynamics of nonequilibrium phonons has become apparent in a variety of experiments in Al_2O_3. Basun, Kaplyanskii, and Shekhtman[1] first pointed to the role of nonresonant Raman scattering of near-zone-boundary phonons in explaining the discrepancy between the results of cw and pulsed laser experiments on the lifetime of 29-cm^{-1} phonons in ruby.[2] Goossens, Dijkhuis, and deWijn[3] confirmed the suggestion of Basun *et al.*, with additional experiments and a detailed analysis. They showed that the nonresonant Raman scattering could even be used as a detector for near-zone-boundary phonons. Engelhardt, Happek, and Renk[4] presented evidence for the inelastic Raman scattering of 891-GHz phonons generated on V^{4+} ions to 874 GHz as detected by hot luminescence from the $2\overline{A}$ level of Cr^{3+}. They attributed the source of the Raman scattering to low-lying resonances of the Cr^{2+} ions present in the samples. The scattering rate was found to decrease after uv irradiation which decreased the Cr^{2+} concentration.[5] Further support for the role of Cr^{2+} was based on the effect of x-ray irradiation to increase the Cr^{2+} concentration, which produced a marked decrease in the lifetime of resonantly generated 29-cm^{-1} phonons.[6] The spectral shift has been successfully analyzed with a model involving spectral-spatial diffusion.[7]

In the experiments described in this paper a monoenergetic nonequilibrium distribution of phonons is generated by ion-lattice relaxation among a pair of excited states of Pr^{3+} ions split by 23 cm^{-1} by the crystal field. The lifetime of the 23-cm^{-1} phonons is reduced by a factor of 5 when the low-lying transitions of co-doped Dy^{3+} ions are brought into resonance with the 23-cm^{-1} phonons by tuning with a magnetic field. We analyze the phonon dynamics with a coupled set of rate equations which include, in addition to the dynamics of the phonons, the dynamics of the ground manifold Dy^{3+} ions and the excited state Pr^{3+} ions.

The effect of a double resonance on the dynamics of phonons is reminiscent of effects observed in level-crossing thermal-conductivity experiments, where peaks were observed in the thermal conductivity when low-lying transitions of two different types of ions were brought into resonance using stress or a magnetic field.[8] In those experiments it was elastic scattering of two energy bands of phonons resonant with the two types of ions which limited the phonon transport. When the transitions on the two types of ions were brought into resonance, there was an increase in the conductivity because then only a single energy band of phonons was scattered. In contrast, in the present experiment when

ground-state transition energies are brought into resonance with the 23-cm^{-1} phonons by a magnetic field, it is inelastic scattering which dominates the phonon dynamics.

II. EXPERIMENTS

The experiments were carried out at a temperature of 1.5 K on a double-doped sample of LaF_3 containing Pr^{3+} (0.05 at. %) and Dy^{3+} (0.01 at %) obtained from Optovac, Inc. The frequency of a pulsed tunable dye laser was tuned to the $^3H_4(1) \rightarrow {}^1D_2(2)$ transition of the Pr^{3+} ion, whose relevant energy levels are shown in Fig. 1. The dye laser consisted of an oscillator with the diffraction grating in a grazing incidence geometry, followed by two amplifiers, all pumped by a frequency-doubled Nd:YAG (where YAG denotes yttrium aluminum garnet) laser. The output of the dye laser at 5917 Å produced a 6-nsec, 0.4-mJ pulse of bandwidth 0.3 cm^{-1}. The π polarized laser beam was focused so as to excite an 800-μm-diameter cylinder in the crystal. Rapid relaxation among the $^1D_2$ levels ($2 \rightarrow 1$), with $T_1 = 225$ psec, generated a monoenergetic phonon distribution whose occupation number was $\bar{p} \cong 0.1$.

The 23-cm^{-1} phonons undergo strong resonant absorption by the excited Pr^{3+} ions. As a result, they are resonantly trapped in the excited volume and give rise to hot luminescence from the $^1D_2(2)$ level, the intensity of which is proportional to the occupation number of the 23-cm^{-1} phonons. The temporal behavior of the phonon occupation was obtained from the time dependence of the hot luminescence viewed at right angles from the laser propagation direction. The luminescence was focused onto the 400-μm-wide slits of a 0.75-m Spex monochrometer and was detected with a photomultiplier whose temporal profile was digitized using a Biomation 6500 transient digitizer. The information was signal averaged on a computer using the data from approximately 1000 laser pulses.

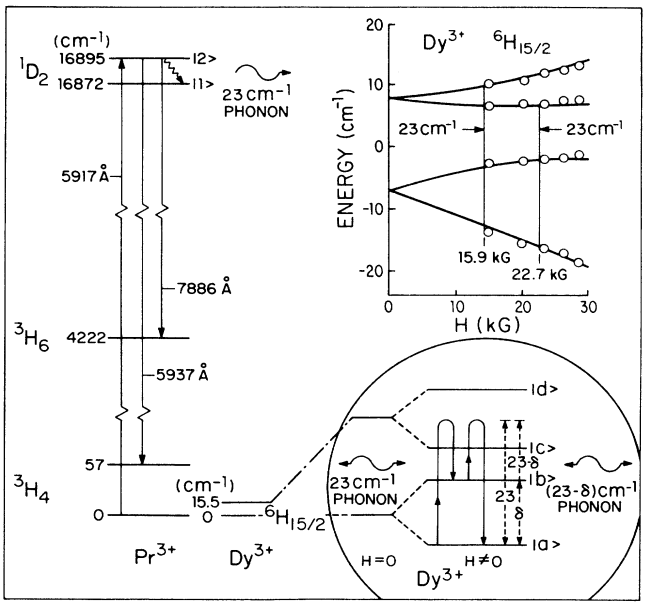

FIG. 1. Energy-level diagram for Pr^{3+} and Dy^{3+} in LaF_3 in zero magnetic field (left) and for Dy^{3+} in the presence of a magnetic field (right). The inset in the upper right shows the Zeeman effect for the two lowest crystal-field levels of Dy^{3+}. The open circles are experimentally obtained from fluorescence. The solid curves are calculated as described in Sec. III. The Pr^{3+} levels are independent of magnetic field. The expanded energy-level diagram for Dy^{3+}, in the lower right, indicates the various phonon Raman scattering processes.

We investigated the time dependence of the hot luminescence in both a single-doped sample (0.05 at. % Pr^{3+}) and the double-doped sample as a function of magnetic field from 0–30 kG along the c axis. The energy levels of the Pr^{3+} ions are independent of field. The magnetic field dependence of the energies of the low-lying Dy^{3+} levels were determined by fluorescence measurements originating from the $^4F_{9/2}$ metastable Dy^{3+} excited state and are shown in Fig. 1. Transitions $|a\rangle \rightarrow |d\rangle$ and $|a\rangle \rightarrow |c\rangle$ are resonant with the 23-cm^{-1} phonons at 15.9 and 22.7 kG, respectively. Under resonant conditions a fraction of the phonons which are absorbed by transitions $|a\rangle \rightarrow |c\rangle$ or $|a\rangle \rightarrow |d\rangle$ undergo inelastic scattering by an amount of energy δ leaving the Dy^{3+} ion in level $|b\rangle$.

III. TIME-RESOLVED RESULTS

When the $^1D_2(2)$ level of Pr^{3+} in LaF_3 is optically pumped in the single-doped sample (0.05 at. % Pr^{3+}), the resulting hot luminescence originating from the $^1D_2(2)$ level decays exponentially with a decay time of $T = 590$ nsec. This, we believe, represents the anharmonic decay time T_{anh} of the 23-cm^{-1} phonons which maintain the population of the $^1D_2(2)$ state.[9] T_{anh} is independent of the excited Pr^{3+} concentration N^*_{Pr}, the diameter of the excited volume, and the Pr^{3+} concentration in the range of 0.002 at. % to 0.05 at. %.

When the experiment is repeated in the double-doped sample at zero magnetic field, nearly the same lifetime ($\tau = 600$ nsec) is obtained. However, at magnetic fields of 15.9 and 22.7 kG, when the 23-cm^{-1} phonons are resonant with transitions within the Dy^{3+} ground manifold, the hot luminescence decays much more rapidly.

The time dependence of the hot luminescence at several magnetic fields is shown in Fig. 2. The long tails of the hot luminescence arise in part from a slight heating of the excited volume by the laser beam, since they are seen even in the single-doped samples. We believe that the excited volume reaches a quasiequilibrium temperature which cools on a microsecond time scale. The initial relaxation rate of the hot luminescence as a function of magnetic field is summarized in Fig. 3. For convenience, the abcissa also indicates the energy splittings between level $|a\rangle$ and the levels $|d\rangle$ (Δ_{ad}) and $|c\rangle$ (Δ_{ac}) of Dy^{3+}, obtained from Fig. 1. Note the two peaks at 15.9 and 22.7 kG which occur when Δ_{ad} and Δ_{ac} equal the phonon energy of 23 cm^{-1}. The peak heights are in the ratio of 2.5 and their half-widths are 1.0 and 1.4 cm^{-1}, respectively. We interpret the

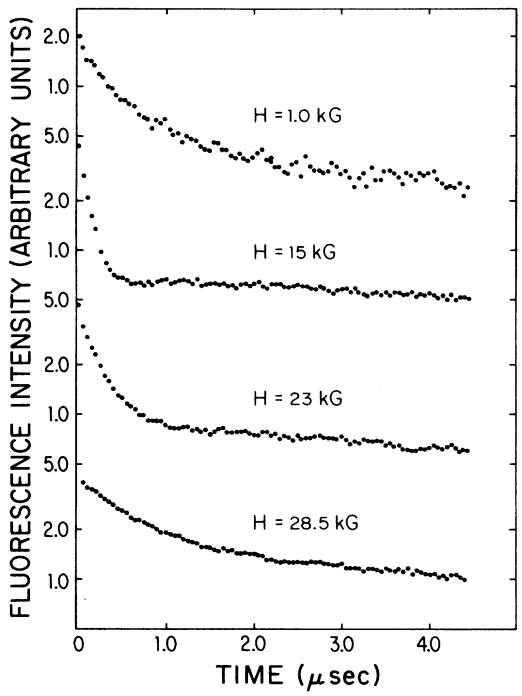

FIG. 2. Temporal dependence of the hot luminescence from the Pr^{3+} $^1D_2(2)$ level at several magnetic fields. These focal-spot-size pulse energy data were obtained by focusing 0.5 mJ on an 800 μm focal diameter.

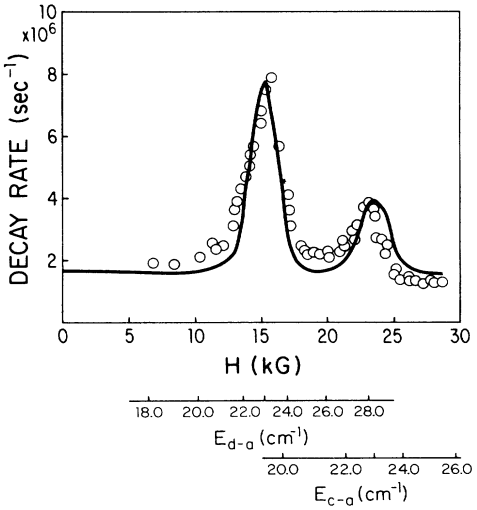

FIG. 3. Decay rate of the hot luminescence in the initial fast-decay time domain (defined in the text) as a function of magnetic field. The energy splittings Δ_{ad} and Δ_{ac} of the Dy^{3+} ions as a function of magnetic field are indicated below the figure. The open circles are the data and the solid curve is a fit to the data with the model described in Sec. III.

enhanced decay as resulting from resonant Raman scattering, whereby the 23-cm^{-1} phonons are inelastically scattered to an energy of $23-\delta$ cm^{-1} by the Dy^{3+} ions.

The decay rates of the long tails in the double-doped sample are reduced near the resonant fields of 15.9 and 22.7 kG. We explain this by trapping of the $(23-\delta)$-cm^{-1} phonons which are resonantly scattered from $23-\delta$ back to 23 cm^{-1} by Dy^{3+} ions in state $|b\rangle$, thereby maintaining the 23-cm^{-1} phonon population above its thermal equilibrium value until the $(23-\delta)$-cm^{-1} phonons decay inelastically, or diffuse out of the excited volume.

The temporal dependence of the hot luminescence can be separated into four distinct time domains. In the first, rapid spin-lattice lattice relaxation from the Pr^{3+} $^1D_2(2)$ state to the $^1D_2(1)$ state, generating 23-cm^{-1} phonons, leads to a rapid (<1 nsec) initial decrease in the luminescence intensity by a factor of about 200, after which phonon trapping takes place. This relaxation is not observed with the time resolution available in these experiments. Subsequent decay of the hot luminescence during the second time domain, referred to as the initial fast decay, is governed by the dynamics of 23-cm^{-1} phonons. During this time domain, which lasts about 1.0 μsec, the decay is dominated by either anharmonic breakup of the nonequilibrium 23-cm^{-1} phonons at magnetic fields far removed from 15.9 and 22.7 kG, or resonant Raman scattering near these two resonant fields.

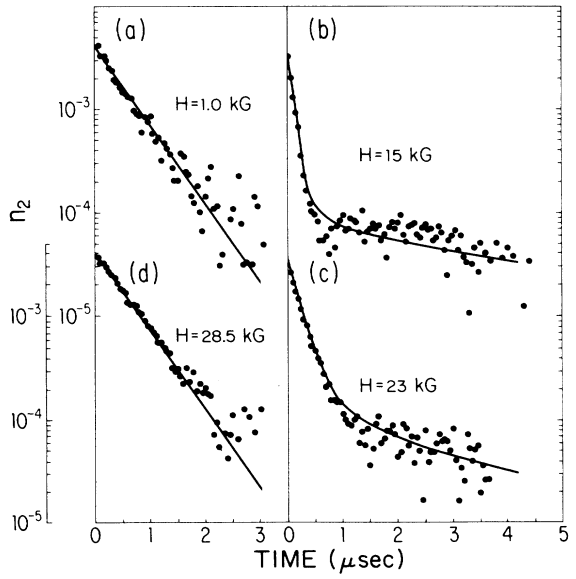

FIG. 4. Temporal dependence of the relative population of the Pr^{3+} $^1D_2(2)$ level ($n_2=N_2/N_{Pr}^*$) at several magnetic fields after the long tails shown in Fig. 2 have been subtracted. The experimental values of n_2, shown as solid circles, are determined by normalizing the fluorescence data in the manner described in Sec. IV. The solid curves are the results of the model calculations as outlined in Sec. IV.

The long tails in the hot luminescence shown in Fig. 2 which constitute the fourth time domain are attributed to the heating caused by the laser pulse with decay times from 10 to 25 μsec. When these long tails are subtracted from the data in a manner described in Sec. IV, the resulting data exhibits the temporal behavior shown in Fig. 4. The solid curves represent the model calculations for the relative population of the Pr^{3+} $^1D_2(2)$ level ($n_2 = N_2/N_{Pr}^*$) described in Sec. IV, and the fluorescence data has been normalized to the model calculations at $t = 10$ nsec. At 15.9 and 22.7 kG, the data exhibits a reduced decay rate for times between 1.0 and 3.0 μsec, the third time domain, which is predicted by the resonant Raman scattering model. The decay rates shown in Fig. 3 were obtained from the data after these long tails were subtracted in order to show more clearly the dynamics in this third time domain.

The source of the heating is uncertain. One possibility is surface absorption of a small portion of the laser beam with the subsequent diffusion of the resulting heat pulse into the bulk of the crystal.[10] Another possibility, based on our earlier observation[11] in single-doped LaF_3:Pr^{3+}, for Pr^{3+} concentrations of 0.1% and 0.5% is that upconversion to the $^3P_0$ state of Pr^{3+}, followed by rapid nonradiative relaxation, can lead to significant generation of high-frequency phonons. Residual upconversion at the reduced Pr^{3+} concentration used in these studies could generate enough 23- and $(23-\delta)$-cm^{-1} phonons by anharmonic decay of the high-frequency phonons to produce the observed enhanced fluorescence in the fourth time domain.

IV. ANALYSIS

A. Rate equations

We present below a rate equation model which takes into account the time dependence of the single phonon process between the two excited states of Pr^{3+}, the Raman shifting of the 23-cm^{-1} phonons involving the ground manifold states of Dy^{3+}, and the single-phonon process between the two lowest states of the Dy^{3+} ground manifold. The rate equations which account for these processes, including the diffusive escape of the 23-cm^{-1}, $(23-\delta)$-cm^{-1}, and δ-cm^{-1} phonons out of the excited volume, can be written as

$$\frac{dn_1}{dt} = T_{1,Pr}^{-1}[n_2(1+\bar{p}_{23}) - n_1\bar{p}_{23}] , \tag{1a}$$

$$\frac{dn_2}{dt} = -\frac{dn_1}{dt} , \tag{1b}$$

$$\frac{d\bar{p}_{23}}{dt} = \frac{N_{Pr}^*}{\Sigma_{23}}\frac{dn_1}{dt} - T_{anh}^{-1}(23)\bar{p}_{23} - T_d^{-1}(23)\bar{p}_{23} - \frac{N_{Dy}}{\Sigma_{23}}(W_{R,up} - W_{R,down}) , \tag{1c}$$

$$\frac{dn_a}{dt} = T_{1,Dy}^{-1}[n_b(1+\bar{p}_\delta) - n_a\bar{p}_\delta] - (W_{R,up} - W_{R,down}) , \tag{1d}$$

$$\frac{dn_b}{dt} = -\frac{dn_a}{dt} , \tag{1e}$$

$$\frac{d\bar{p}_{23-\delta}}{dt} = \frac{N_{Dy}}{\Sigma_{23-\delta}}(W_{R,up} - W_{R,down}) - T_d^{-1}(23-\delta)\bar{p}_{23-\delta} - T_{ahn}^{-1}(23-\delta)\bar{p}_{23-\delta} , \tag{1f}$$

$$\frac{d\bar{p}_\delta}{dt} = \frac{N_{Dy}}{\Sigma_\delta}T_{1,Dy}^{-1}[n_b(1+\bar{p}_\delta) - n_a\bar{p}_\delta] - T_d^{-1}(\delta)\bar{p}_\delta - T_{anh}^{-1}(\delta)\bar{p}_\delta . \tag{1g}$$

The electronic state populations $n_{1(2)} = N_{1(2)}/N_{Pr}^*$ and $n_{a(b)} = N_{a(b)}/N_{Dy}$ refer to the states in Fig. 1. The phonon occupation numbers $\bar{p}_{23}$, $\bar{p}_{23-\delta}$, and $\bar{p}_\delta$ refer to the three pertinent phonon groups indicated in Fig. 1. Σ_{23}, $\Sigma_{23-\delta}$, and Σ_δ are the total number of phonon modes contained in the electronic resonance bandwidths. $T_{1,Pr}^{-1}$ and $T_{1,Dy}^{-1}$ are the single-phonon relaxation rates between levels $|1\rangle$ and $|2\rangle$, and $|a\rangle$ and $|b\rangle$, respectively, and $T_{anh}^{-1}(23)$ is the anharmonic decay rate (1.6×10^6 sec^{-1}) of the 23-cm^{-1} phonons. $T_{anh}^{-1}(x)$ are the anharmonic decay rates of the $x = \delta$ and $(23-\delta)$-cm^{-1} phonons, obtained by scaling the rate for the 23-cm^{-1} phonons by the fifth power of the frequency.[12] The $T_d^{-1}(x)$ are the diffusion loss rates of the phonons out of the volume based on a mean free path limited by elastic defect scattering, elastic and inelastic Raman scattering, and resonant single-phonon scattering, and are given by

$$T_d^{-1}(x) = (v/R)^2(\Sigma_i \tau_{s,i}^{-1})^{-1} , \tag{2}$$

where v is the group velocity of the phonons, R is the radius of the excited volume, and $\tau_{s,i}^{-1}$ ($i = 1,2,3$) are the scattering rates for the above three processes. All three terms are included for the 23-cm^{-1} phonons. However, there is no resonant single-phonon process for the $(23-\delta)$-cm^{-1} phonons and no Raman scattering terms for the δ-cm^{-1} phonons.

The rate $W_{R,up}$ describes the sum of all inelastic Raman processes inducing transitions $|a\rangle \rightarrow |b\rangle$. The rate $W_{R,down}$ describes the reverse Raman processes. For instance

$$W_{R,up} = (W_{a\rightarrow d\rightarrow b} + W_{a\rightarrow c\rightarrow b})/N_{Dy} , \tag{3}$$

$$W_{R,down} = (W_{b\rightarrow d\rightarrow a} + W_{b\rightarrow c\rightarrow a})/N_{Dy} . \tag{4}$$

In order to describe the time dependence of the relaxation process in the presence of a nonequilibrium phonon population we refer to Orbach's original treatment of spin relaxation,[13] in which the probability per unit time for the transition $|a\rangle \rightarrow |d\rangle \rightarrow |b\rangle$ is given by

$$W_{a\rightarrow d\rightarrow b} = C_d \int \frac{1}{(\hbar\omega - \Delta_{ab})^2} \times \omega^3(\omega - \delta/\hbar)^3 \bar{p}'(\bar{p}+1)N_a\, d\omega , \tag{5}$$

where

$$C_d = \frac{9}{8\pi^3\rho^2 v^{10}} \left| \sum_{\substack{n,m \\ n',m'}} \langle a | V_n^m | d \rangle \langle d | V_{n'}^{m'} | b \rangle \right|^2 . \tag{6}$$

and where $\omega(\omega-\delta/\hbar)$ is the incident (emitted) phonon frequency, Δ_{ad} is the energy difference between the states $|a\rangle$ and $|d\rangle$,$\bar{p}'$ ($\bar{p}$) is the phonon occupation number of the incident (emitted) phonons, and N_a is the electronic population of the $|a\rangle$ state. Similar expressions for $W_{b\to d\to a}$, $W_{a\to c\to b}$, and $W_{b\to c\to a}$ follow by interchanging the appropriate indices.

In the present case none of the usual low-temperature, low magnetic field approximations are valid, so the integrals must be evaluated exactly (numerically) through the resonant conditions. In addition, within the range of magnetic fields of primary interest in this work, selection rules due to Kramer's theorem are relaxed due to the large mixing between the four Dy^{3+} Zeeman components. This is evident from the nonlinear splitting of these states as seen in Fig. 1. Hence, we will follow the treatment for non-Kramer's ions.

The energy denominators of Eq. (5) are evaluated according to the technique of Orbach,[13] by adding a term $i\Gamma_{Hd}/2$ yielding

$$|ED(\omega)|^2=\left|\frac{1}{\hbar\omega-\Delta_{ad}+i\Gamma_{Hd}/2}\right|^2 =\frac{1}{(\hbar\omega-\Delta_{ad})^2+\Gamma_{Hd}^2/4}\ , \tag{7}$$

where Γ_{Hd} is the homogeneous linewidth of the $|a\rangle\leftrightarrow|d\rangle\leftrightarrow|b\rangle$ resonance given by[13]

$$\Gamma_{Hd}=\frac{3}{2\pi\rho v^5}\left[\left(\frac{\Delta_{ad}}{\hbar}\right)^3\left|\sum_{n,m}\langle a|V_n^m|d\rangle\right|^2(\bar{p}+1) +\left(\frac{\Delta_{bd}}{\hbar}\right)^3\left|\sum_{n',m'}\langle d|V_{n'}^{m'}|b\rangle\right|^2(\bar{p}'+1)\right]. \tag{8}$$

Γ_{Hc} is given by a similar expression for the $|a\rangle\leftrightarrow|c\rangle\leftrightarrow|b\rangle$ resonance.

The Pr^{3+} $|2\rangle\leftrightarrow|1\rangle$ and the Dy^{3+} $|a\rangle\leftrightarrow|d\rangle$, etc., resonances are inhomogeneously broadened. As a result, we must consider a distribution of phonon frequencies centered at 23 cm^{-1} of half-width Γ_{Pr} interacting with a distribution of Dy^{3+} ions whose resonance frequency is centered at Δ_{ad} and whose half-width is Γ_d. The integral in Eq. (5) is evaluated in two steps. First, we consider a given subset of Dy^{3+} ions whose resonance $|a\rangle\leftrightarrow|d\rangle$ occurs at a frequency ω', with homogeneous width Γ_{Hd}. We now integrate over the 23-cm^{-1} phonon width Γ_{Pr} to obtain a scattering rate for those ions

$$W_{a\to d\to b}(\omega')=C_d\int_{\Gamma_{Pr}}|ED(\omega)|^2(\omega-\delta/\hbar)^3\omega^3N_a \times\bar{p}_{23}(\bar{p}_{23-\delta}+1)d\omega\ . \tag{9}$$

Then an integral over the distribution of Dy^{3+} sites with inhomogeneous linewidth Γ_d produces

$$W_{a\to d\to b}=\int_{\Gamma_d}P_{\text{Gauss}}(\omega')W_{a\to d\to b}(\omega')d\omega'\ . \tag{10}$$

A similar expression for $W_{a\to c\to b}$ is obtained by substituting the state $|c\rangle$ for state $|d\rangle$ in all the above expressions. The rate equations are now solved numerically to produce the time dependences of the electronic state populations and the phonon occupation numbers.

B. Parameters

There are a number of parameters in this model which must be determined or estimated. These include, for the Dy^{3+} ions, the matrix elements (M_{ij}) for the Raman processes (electron-phonon matrix elements), the homogeneous (Γ_H) and inhomogeneous (Γ_i) linewidths for the Dy^{3+} ground-state resonances, and the Dy^{3+} single-phonon relaxation rate between the $|a\rangle$ and $|b\rangle$ states ($T_{1,\text{Dy}}^{-1}$). For the Pr^{3+} ions we require the single-phonon relaxation rate between the lowest two states of the $^1D_2$ manifold ($T_{1,\text{Pr}}^{-1}$), which is well known, the inhomogeneous linewidth for this resonance (Γ_{Pr}), which determines the width of the 23-cm^{-1} phonon distribution, and the density of excited state Pr^{3+} ions. For the phonons we need the anharmonic phonon decay rates [$T_{\text{anh}}^{-1}(\omega)$], the elastic defect scattering rates [$T_d^{-1}(\omega)$] for the three phonon groups, and an estimate of the phonon density of states [$\rho(\omega)$].

The Pr^{3+} $^1D_2$ ($|2\rangle\leftrightarrow|1\rangle$) relaxation time $T_{1,\text{Pr}}$ is 225 psec, based on the work of Erickson.[14] The inhomogeneous linewidth for this transition, Γ_{Pr}, was found to be 30 GHz in the double-doped sample using a non-resonant fluorescence-line-narrowing (FLN) technique.[15] The inhomogeneous Dy^{3+} linewidths, Γ_d, Γ_c, and Γ_b, were initially assumed to be of the order of 30 GHz, based on the observed optical spectra, but were varied to produce a best fit to the observed widths of the peaks in the phonon decay rates as a function of magnetic field.

Anharmonic decay rates $T_{\text{anh}}^{-1}(x)$ for the three phonon groups are based on the measured decay rate for 23-cm^{-1} phonons of 1.6×10^6 (sec^{-1}) at zero magnetic field in this sample, as well as the almost identical result measured in a single-doped LaF_3:Pr^{3+} sample, scaled by the fifth power of the phonon frequency for the other phonon frequencies.

The elastic defect scattering rates $\tau_{s,\text{def}}^{-1}(\omega)$ were estimated from thermal-conductivity measurements of Dixon[16] to be $\tau_{s,\text{def}}^{-1}=A\omega$ (sec^{-1}), with $A=5.8\times10^{-5}$. The resonant single-phonon scattering rates for the 23- and δ-cm^{-1} phonons are

$$\tau_{s,\text{res}}^{-1}(23)=T_{1,\text{Pr}}^{-1}b_{\text{Pr}}(1+b_{\text{Pr}}) \tag{11}$$

and

$$\tau_{s,\text{res}}^{-1}(\delta)=T_{1,\text{Dy}}^{-1}b_{\text{Dy}}(1+b_{\text{Dy}})\ , \tag{12}$$

where $b_{\text{Pr}}=N_{\text{Pr}}^*/\Sigma_{\text{Pr}}$ and $b_{\text{Dy}}=N_{\text{Dy}}/\Sigma_{\text{Dy}}$.

The excited-state density of Pr^{3+} ions, N_{Pr}^*, was first calculated using the measured absorption coefficient, the laser energy, and the excited volume. During the analysis a better estimate of N_{Pr}^* was obtained by fitting the extent of the initial fast decay (relative decrease in the fluorescence intensity) to the model results, which will be described in more detail in Sec. IV. The phonon density of states $\rho(\omega)$ was taken from calculations of Meltzer *et al.*[17] for 41-cm^{-1} acoustic phonons in LaF_3, scaled by ω^2 to the appropriate phonon energies for this work.

The inelastic Raman scattering rates for the phonons depend on the same matrix elements as the Raman rates for the electronic transitions but in different combinations. For the purpose of the discussion we define

$$M_{ijk}^2 = \left| \sum_{\substack{n,m,\\ n',m'}} \langle i \mid V_n^m \mid j \rangle \langle j \mid V_{n'}^{m'} \mid k \rangle \right|^2 , \tag{13}$$

where i, j, and k stand for the states $|a\rangle$, $|b\rangle$, $|c\rangle$, and $|d\rangle$. The elastic Raman rates are proportional to the matrix elements M_{ada}^2 and M_{aca}^2 for the 23-cm^{-1} phonons and M_{bdb}^2 and M_{bcb}^2 for the $(23-\delta)$-cm^{-1} phonons. In addition, the direct process rate for the $|a\rangle$ to $|b\rangle$ resonance is proportional to

$$M_{ab}^2 = \left| \sum_{n,m} \langle a \mid V_n^m \mid b \rangle \right|^2 ,$$

while the homogeneous linewidths for the Raman resonances are given by Eq. (8). For the purposes of this analysis we assume $M_{ijk}^2 = M_{ij}^2 M_{jk}^2$.

The values of the matrix elements are strongly magnetic field dependent, which further complicates the problem of analyzing the field dependence of the phonon dynamics. Their field dependence affects both the scattering rates among the three phonon packets and, to a lesser extent, the mean free path of the phonons which determines their escape time from the excited volume. However, it is possible to calculate the field dependence of the matrix elements once the zero-field matrix elements, spin-flip ($\mathcal{M}_{SF}$) and spin-non-flip ($\mathcal{M}_{SNF}$), are known, and thus it is only these which must be specified as input parameters.

The magnetic field dependence of the ion-phonon matrix elements is obtained as follows. First, the eigenstates of the four states comprising the two low-lying Kramer's pairs of states for Dy^{3+} are obtained as a function of magnetic field. The 4×4 matrix of the energy Hamiltonian containing the crystal-field energies and Zeeman energies is diagonalized in a basis set containing two pairs of Kramer's conjugate states quantized along the magnetic field direction (c axis). The Zeeman part of the matrix contains as parameters the splitting factors s and s' for the lowest and first excited crystal-field states, respectively, and two independent off-diagonal Zeeman matrix elements coupling the basis states. The two components within each Kramer's pair are not coupled by the field.

Although the matrix is in general complex, the off-diagonal matrix elements are chosen to be real since this has no effect on the eigenvalues. Whereas this does affect the ion-phonon matrix elements which are also complex, it is sufficient in our numerical analysis to simply determine one phase factor for each matrix element in the real zero-field basis, obtained by fitting the experimental results to the theory.

Labeling the basis states as $|1\rangle$, $|2\rangle$, $|3\rangle$, and $|4\rangle$, in order of ascending energy at low fields, we find a best fit to the observed energies with the following parameters. The zero-field splitting is $\Delta = 14.8$ cm^{-1}, the splitting factors of the two low-lying crystal-field states of Dy^{3+} are $s = 14.5$ and $s = 5$, and the off-diagonal Zeeman matrix elements are $\langle 1 \mid H_{Zeeman} \mid 4 \rangle = 5$ cm^{-1} and $\langle 1 \mid H_{Zeeman} \mid 3 \rangle = 4$ cm^{-1}. The resulting fit is excellent, as seen in Fig. 1, where the observed energy levels (open circles) are compared with the diagonalization results (solid curves) as a function of magnetic field.

We varied the unknown and uncertain parameters until best fits were obtained for the 23-cm^{-1} phonon decay rate as a function of magnetic field. In the vicinity of the enhanced 23-cm^{-1} phonon decay rates at 15.9 and 22.7 kG, the time dependence of the fast early time decay was determined by the products of the squares of the appropriate ion-phonon matrix elements and the associated homogeneous linewidths for the Raman resonances. Near 15 kG the $|a\rangle \leftrightarrow |d\rangle \leftrightarrow |b\rangle$ Raman process was mainly responsible for the initial decay (125 nsec), while near 23 kG the $|a\rangle \leftrightarrow |c\rangle \leftrightarrow |b\rangle$ Raman process dominated the initial decay (250 nsec).

The fast Raman processes generate a nonequilibrium population of $(23-\delta)$-cm^{-1} phonons as well as a nonequilibrium population of the Dy^{3+} $|b\rangle$ state. Thereafter, the "reverse" Raman processes, ($|b\rangle \rightarrow |d\rangle \rightarrow |a\rangle$ or $|b\rangle \rightarrow |c\rangle \rightarrow |a\rangle$), whereby a $(23-\delta)$-cm^{-1} phonon is annihilated and a 23-cm^{-1} phonon is created, causes a steady-state balance in the creation and annihilation of the 23-cm^{-1} phonons. Further loss in the 23-cm^{-1} phonon population is governed by anharmonic decay and by the diffusive loss of the $(23-\delta)$-cm^{-1} phonons out of the excited volume. This produces the slowly decaying luminescence tails during the third time domain seen in Fig. 4 for magnetic fields near the 15.9 and 22.7 kG resonances. Off resonance, the Raman process rates are much too slow to produce significant populations of $(23-\delta)$-cm^{-1} phonons, so the decay is interpreted as representing the anharmonic decay time of the 23-cm^{-1} phonons (600 nsec).

So far the analysis has been carried out in order to fit the data displayed in Fig. 4. The effect of the heating which is evidenced in the raw data in Fig. 2 during the fourth time domain has been ignored. At this point, it is possible to at least partially analyze the effect of the small heat pulse, which is always present, on the data.

At low magnetic fields and for fields well above 22.7 kG the long tails (decay times of 10 μsec) most probably represent the net decay time of the 23-cm^{-1} phonons produced in the original heat pulse. When this is subtracted from the data at 1.0 and 28.5 kG the 600 nsec decays shown in Figs. 4(a) and 4(d) are obtained.

The data in Figs. 2(b) and 2(c) exhibit decay times of 25 and 15 μsec at 15.9 and 22.7 kG, respectively. Thus the net loss rate of the 23-cm^{-1} phonons is reduced significantly for fields where the resonant Raman process is important.

If the net loss rate of the 23-cm^{-1} phonons due to the heat pulse is 10 μsec off resonance, then it follows that the anharmonic decay products at about 10–15 cm^{-1} should increase in population with a characteristic time of about 10 μsec. At 15.9 kG the population of the $(23-\delta)$-cm^{-1} phonons should therefore increase in time due to the heat pulse with a buildup time of $\simeq 10$ μsec. This in turn would lead to an enhanced 23-cm^{-1} phonon population due to Raman scattering of the $(23-\delta)$-cm^{-1}

phonons. Using our model calculations, with the inclusion of a buildup of the $(23-\delta)$-cm^{-1} phonons, it was possible to obtain an increased decay time for the 23-cm^{-1} phonons at 15.9 kG of 25 μsec. However, lacking a detailed model for the approach to equilibrium of the high-frequency phonons generated in the heat pulse, it is not possible to make a quantitative estimate of the long-time behavior of the 23-cm^{-1} phonons in the presence of the heat pulse.

Instead, the following approach was taken. The observed fluorescence in the fourth time domain at each value of the magnetic field shown in Fig. 2 was subtracted from the data in order to produce the results shown in Fig. 4. The parameters in the model calculations were then fit to the data of Fig. 4. The calculated fluorescence intensity was normalized to the Pr^{3+} $^1D_2(2)$ state population as determined in the model calculations at a time of 0.01 μsec.

The magnitudes of the 23-cm^{-1} phonon decay rates near 15.9 and 22.7 kG could be fit equally well for values of the ratio of the zero-field spin-flip to spin-non-flip ($\mathcal{M}_{SF}/\mathcal{M}_{SNF}$) ion-phonon matrix elements ranging from about $\frac{1}{2}$ to 3 by choosing an appropriate phase angle. We arbitrarily use a value of $\mathcal{M}_{SF}/\mathcal{M}_{SNF}$ of 2 in the succeeding discussion of the fit to the data. This choice yields values of $\mathcal{M}_{SF}=100$ cm^{-1} and $\mathcal{M}_{SNF}=50$ cm^{-1} at $H=0$. By way of comparison it is noted that Schultz and Jeffries[18] found that values of the matrix elements between crystal levels of the ground manifolds in a number of rare-earth ions in LaF_3 would have to range from about 150 to 500 cm^{-1} in order to explain their spin-lattice relaxation data. Earlier, Scott and Jeffries[19] calculated these matrix elements for several rare-earth ions in the double nitrates and ethyl sulfates and obtained values ranging from 10 to 120 cm^{-1}.

The best fit to the field dependence of the decay rates is given by the solid curve in Fig. 3. The widths of the two peaks depend on Γ_{Pr}, which determines the frequency width of the 23-cm^{-1} phonon distribution, and the inhomogeneous linewidths of the Dy^{3+} $|a\rangle\leftrightarrow|d\rangle\leftrightarrow|b\rangle$ (15.9 kG) and $|a\rangle\leftrightarrow|c\rangle\leftrightarrow|b\rangle$ (22.7 kG) Raman resonances. These were varied to produce the fits to the width of the peaks shown in Fig. 3. The best-fit values of the linewidths are listed in Table I, along with the best values of the other parameters.

The magnetic field dependence of the ion-phonon matrix elements used for the Raman rate calculations is displayed in Fig. 5. The strong field dependence, mentioned above, is clearly evident.

We calculated the diffusive mean free paths for defect scattering, resonant single-phonon scattering, and elastic and inelastic Raman scattering, using the best-fit results. The magnetic field dependence of these mean free paths is shown in Fig. 6, where it is evident that the defect and resonant single-phonon scattering are the main processes which limit the diffusive loss of the three phonon groups. Contrary to our original expectations that resonant single-phonon scattering would control the diffusion of the 23-cm^{-1} phonons, defect scattering is found to be at least as important.

Our model analysis indicates that the decay time of the long tails observed in the time dependence of the fluorescence between 1.0 and 3.0 μsec (time domain three) is strongly influenced by the diffusive loss rate of the $(23-\delta)$-cm^{-1} phonons. Near 15 kG the 10-μm mean free path of the $(23-\delta)$-cm^{-1} phonons (see Fig. 6) leads to a diffusive time for escape from the 800 μm excited volume radius of $\simeq 10$ μsec. Thus, near 15.9 and 22.7 kG, where the resonant Raman process creates a sizable population of $(23-\delta)$-cm^{-1} phonons ($\bar{p}\simeq 0.03$)

TABLE I. Parameters used to fit the experimental data.

Parameter	Value	Source
	Parameters independent of ion-phonon matrix elements	
N^*_{Pr}	0.5×10^{17} cm^{-3}	Calculated and fit to initial fast decay
N_{Dy}	1.6×10^{18} cm^{-3}	Calculated
$T_{anh}(23)$	600 nsec	Measured
Σ_{41}	$5\times10^{+19}$ cm^{-3} per cm^{-1}	a
$T^{-1}_{1,Pr}$	0.45×10^{10} sec^{-1}	b
$\tau^{-1}_{s,def}(23)$	2.5×10^{8} sec^{-1}	c
Γ_{Pr}	1.0 cm^{-1}	Measured
Γ_d	1.0 cm^{-1}	Fit to decay peak width at 15 kG
Γ_c	0.5 cm^{-1}	Fit to decay peak width at 23 kG
Γ_b	0.25 cm^{-1}	Estimated
	Parameters dependent on ion-phonon matrix elements	
$M_{ad}(H=0)$	50 cm^{-1}	Normalized to fit fast decay near 15 kG
$M_{bd}(H=0)$	100 cm^{-1}	Normalized to fit fast decay near 23 kG
$\Gamma_{Hd}(H=0)$	3×10^{-3} cm^{-1}	Calculated from matrix elements
$\Gamma_{Hc}(H=0)$	3×10^{-3} cm^{-1}	Calculated from matrix elements
$T^{-1}_{1,Dy}(H=1$ kG)	1.0×10^{2} sec^{-1}	Calculated from matrix elements[d]

[a]From Ref. 17.
[b]From Ref. 14.
[c]Calculated from Ref. 16.
[d]See Ref. 18 for comparison.

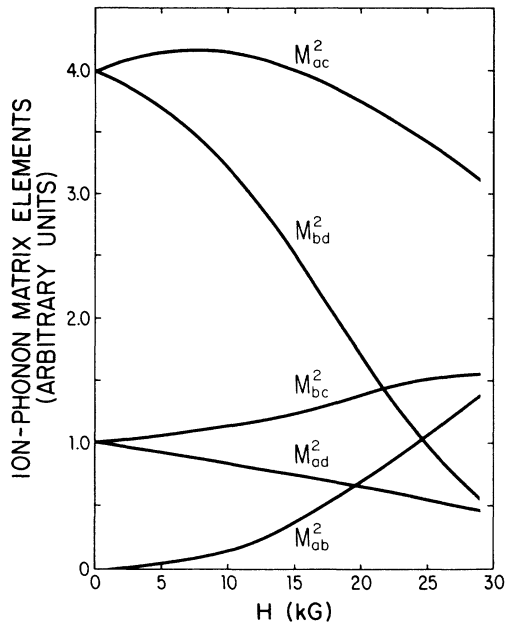

FIG. 5. Magnetic field dependence of the Dy^{3+} ion-phonon matrix elements used in the Raman rate calculations. M^2_{ij} is the square of the matrix element coupling the ith to the jth state.

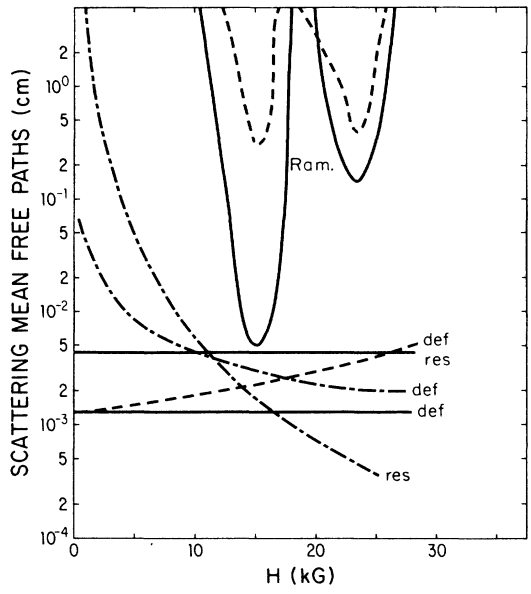

FIG. 6. Calculated values of the Raman (Ram.), defect (def), and resonant (res) scattering mean free paths for the three phonon groups as a function of magnetic field. The parameters used in the calculation are the results of a best fit shown in Fig. 3. The solid curves (——), dashed curves (— — —), and the dash-dotted curves (—·—·—·) correspond to the 23-cm^{-1}, $(23-\delta)$-cm^{-1}, and $\delta-cm^{-1}$ phonon groups, respectively.

and Dy^{3+} ions in excited state $|b\rangle$ ($n_b \simeq 0.07$), the $(23-\delta)$-cm^{-1} phonons recreate 23-cm^{-1} phonons through the $|b\rangle \rightarrow |d\rangle \rightarrow |a\rangle$ or $|b\rangle \rightarrow |c\rangle \rightarrow |a\rangle$ Raman processes, leading to an increased decay time for the 23-cm^{-1} phonons of $\simeq 2$ μsec near 15 kG, and $\simeq 1.4$ μsec near 23 kG, as compared to the anharmonic lifetime of $\simeq 600$ nsec.

When the defect scattering rate of the three phonon groups is reduced by a factor of 100, the calculations indicate that there is no slowly decaying tail and the 23-cm^{-1} phonons continue to decay at the anharmonic rate. When the defect scattering rate is increased by a factor of 10, 23-cm^{-1} phonons exhibit decay times of $\simeq 9.0$ μsec near 15 kG and $\simeq 3.0$ μsec near 23 kG, which are considerably longer than the observed times. It should be pointed out that the defect scattering rates calculated from Dixon's thermal-conductivity data[16] are probably only accurate to within a factor of 2, so that we can only conclude that the calculated scattering rates are consistent with the present data.

When the 23-cm^{-1} phonon bottleneck factor $b = N^*_{Pr}/\Sigma_{Pr}$ ($\simeq 10^{-2}$ in this experiment) is increased, the values of n_2 and $\bar{p}_{23}$ immediately after bottlenecking occurs ($t \simeq 1$ nsec) increase in proportion to b, since for $b < 0.1$ the initial bottlenecked values of n_2 and $\bar{p}$ are known to be approximately equal to b.[20] It is found that decreasing the value of b leads to a larger decrease in n_2 and $\bar{p}_{23}$ prior to the onset of the slower 2.0 μsec decays. Thus, by comparing the extent of this initial fast decay calculated from the model with the experimental data in this second time domain, we are able to determine the value of N^*_{Pr} with somewhat more accuracy than the values estimated as discussed in Sec. III. However, the differences are only a factor of 2.

An increase in N_{Dy} leads to a faster Raman scattering rate which, in turn, yields a faster initial decay rate for magnetic fields near 15.9 and 22.7 kG, as expected.

The best solutions of the coupled rate equations for several magnetic fields are compared with the experimental data in Fig. 4. The time dependence of n_2 is shown for $H = 0$, 15.9, 22.7, and 28.5 kG, where the solid curves represent the best fit to the data.

The values of all the parameters used in the model are listed in Table I. The magnitudes of the ion-phonon matrix elements involving transitions between the various Dy^{3+} states are all determined once the zero-field spin flip and spin-non-flip matrix elements are found by fitting to the initial fast decay at 15.9 and 22.7 kG. It is of interest to note that the calculated value of $T^{-1}_{1,Dy}$, which depends on M_{ab}, is consistent with the experimental results of Schultz and Jeffries[18] for fields of 1.2 kG (although H was perpendicular to the c axis), with a scaling of the relaxation rate by H^5 as predicted for the direct process in Kramer's ions. This is further evidence that our calculated values of the ion-phonon matrix elements are quite reasonable.

V. CONCLUSIONS

The lifetime of 23-cm^{-1} phonons in LaF_3 is reduced from 600 nsec to as little as 125 nsec when the transi-

tions within the $^6H_{15/2}$ ground manifold of Dy^{3+} are tuned with a magnetic field into resonance with the 23-cm^{-1} phonons. Although some of the parameters of the model are not well known, the quality of the fit to the data with reasonable values of these parameters demonstrates that the reduced lifetime results from inelastic Raman scattering of the 23-cm^{-1} phonons to lower energy by an amount equal to the energy difference between the two lowest Dy^{3+} levels.

Experiments which measure the time dependence of the population of the Dy^{3+} $|b\rangle$ state could further test our model for the role of resonant Raman processes.

Although it is generally recognized that the Raman process is an important spin-lattice relaxation mechanism governing the dynamics of the populations of electronic spin states above liquid-helium temperatures (1.5 K), we have shown that this process can also dominate the phonon decay for those phonons which are resonant with transitions within an impurity ion. Thus the lifetime obtained in an experiment which monitors the temporal behavior of the population of a monochromatic distribution of phonons can be greatly affected when these phonons are resonant with transitions of the impurity ion. In the present case, the lifetime was reduced by inelastic Raman scattering of the phonons from the Dy^{3+} impurity ions. However, even at longer times, the resonant phonon population is held up by inelastic Raman scattering of the initial decay products back to the original frequency.

Resonant Raman scattering can be important even for very low concentrations of impurities. Although our experiment is performed with 0.01 at.% Dy^{3+} impurity ions, our calculations suggest that even for more dilute samples, i.e., an order of magnitude less concentrated, the resonant Raman process cannot be neglected in analyzing the phonon lifetime.

ACKNOWLEDGMENTS

We would like to thank Dave Huber and John Henkel for their assistance in the development of the model for the analysis of the data and George Dixon for providing us with his data prior to publication. In addition, we would like to thank the U. S. Army Research Office for the support of this work under Contract No. DAAG29-82-K-0088.

*Present address: Department of Physics, Emory University, Atlanta, GA.

[1]S. A. Basun, A. A. Kaplyanskii, and V. L. Shekhtman, Zh. Eksp. Teor. Fiz. **82**, 1945 (1982) [Sov. Phys—JETP **55**, 1119 (1982)].

[2]R. S. Meltzer, J. E. Rives, and W. C. Egbert, Phys. Rev. B **25**, 3026 (1982).

[3]R. J. G. Goossens, J. I. Dijkhuis, and H. W. deWijn, J. Lumin. **34**, 19 (1985).

[4]M. Engelhardt, U. Happek, and K. F. Renk, Phys. Rev. Lett. **50**, 116 (1983).

[5]U. Happak, T. Holstein, and K. F. Renk, J. Phys. (Paris) Colloq. **46**, C7-493 (1985).

[6]M. Engelhardt and K. F. Renk, in *Phonon Scattering in Condensed Matter,* edited by W. Eisenmenger *et al.* (Springer-Verlag, Berlin, 1984), pp. 124–126.

[7]U. Happek, T. Holstein, and K. F. Renk, Phys. Rev. Lett. **54**, 2091 (1985); in *Proceedings of the Second International Conference on Phonon Physics,* edited by J. Kollar *et al.* (World Scientific, Singapore, 1985), pp. 461–463.

[8]L. J. Challis, in *Phonon Scattering In Condensed Matter,* edited by W. Eisenmenger *et al.* (Springer-Verlag, Berlin, 1984), pp 2–9 and references therein.

[9]R. S. Meltzer and R. M. Macfarlane, Phys. Rev. B **32**, 1248 (1985).

[10]R. S. Meltzer, J. E. Rives, and D. J. Sox, in *Phonon Scattering in Condensed Matter,* edited by W. Eisenmenger *et al.* (Springer-Verlag, Berlin, 1985), pp. 115–117.

[11]S. S. Yom, Ph. D. dissertation, University of Georgia, 1986.

[12]R. Orbach and L. A. Vredevoe, Physics (NY) **1**, 91 (1964).

[13]R. Orbach, Proc. R. Soc. London, Ser. A **264**, 458 (1961).

[14]L. E. Erickson, Opt. Commun. **15**, 246 (1975).

[15]For a description of this technique, see D. J. Sox, S. Majetich, J. E. Rives, and R. S. Meltzer, J. Phys. (Paris) Colloq. **46**, C7-493 (1985).

[16]G. S. Dixon (private communication). The thermal conductivity of a LaF_3–0.1 at.% Er^{3+} sample exhibits a T^2 temature dependence in the low-temperature limit, and this yields a linear frequency dependence for the defect scattering. The magnitude of the constant A is calculated from the experimental thermal-conductivity data. Earlier measurements by Hudson [J. Phys. C **9**, L39 (1976)] on a pure LaF_3 sample exhibited a similar T^2 dependence.

[17]R. S. Meltzer, J. E. Rives, and G. S. Dixon, Phys. Rev. B **28**, 4786 (1983).

[18]M. B. Schultz and C. D. Jeffries, Phys. Rev. **149**, 270 (1966).

[19]P. L. Scott and C. D. Jeffries, Phys. Rev. **127**, 32 (1962).

[20]J. E. Rives and R. S. Meltzer, Phys. Rev. B **16**, 1808 (1977).